Camelback-shaped band reconciles heavy-electron behavior with weak electronic Coulomb correlations in superconducting TlNi₂Se₂

N. Xu,[1,2,*] C. E. Matt,[1,3] P. Richard,[4,5] A. van Roekeghem,[4,6] S. Biermann,[6,7,8] X. Shi,[1,4] S.-F. Wu,[4] H. W. Liu,[4] D. Chen,[4] T. Qian,[4] N. C. Plumb,[1] M. Radović,[1,9] Hangdong Wang,[10] Qianhui Mao,[10] Jianhua Du,[10] Minghu Fang,[10,11] J. Mesot,[1,2,3] H. Ding,[4,5] and M. Shi[1,†]

[1]*Swiss Light Source, Paul Scherrer Insitut, CH-5232 Villigen PSI, Switzerland*
[2]*Institute of Condensed Matter Physics, École Polytechnique Fédérale de Lausanne, CH-1015 Lausanne, Switzerland*
[3]*Laboratory for Solid State Physics, ETH Zürich, CH-8093 Zürich, Switzerland*
[4]*Beijing National Laboratory for Condensed Matter Physics and Institute of Physics, Chinese Academy of Sciences, Beijing 100190, China*
[5]*Collaborative Innovation Center of Quantum Matter, Beijing, China*
[6]*Centre de Physique Théorique, Ecole Polytechnique, CNRS-UMR7644, 91128 Palaiseau, France*
[7]*Collège de France, 11 place Marcelin Berthelot, 75005 Paris, France*
[8]*Kavli Institute for Theoretical Physics, University of California, Santa Barbara, California 93106, USA*
[9]*SwissFEL, Paul Scherrer Institut, CH-5232 Villigen PSI, Switzerland*
[10]*Department of Physics, Zhejiang University, Hangzhou 310027, China*
[11]*Collaborative Innovation Center of Advanced Microstructures, Nanjing University, Nanjing 210093, China*

Combining photoemission spectroscopy, Raman spectroscopy, and first-principles calculations, we characterize superconducting TlNi₂Se₂ as a material with weak electronic Coulomb correlations leading to a bandwidth renormalization of 1.4. We identify a camelback-shaped band, whose energetic position strongly depends on the selenium height. While this feature is universal in transition metal pnictides, in TlNi₂Se₂ it lies in the immediate vicinity of the Fermi level, giving rise to a pronounced van Hove singularity. The resulting heavy band mass resolves the apparent puzzle of a large normal-state Sommerfeld coefficient [H. Wang *et al.*, Phys. Rev. Lett **111**, 207001 (2013)] in this weakly correlated compound.

The discovery of high-temperature superconductivity in iron-chalcogenide $A_x\text{Fe}_{2-y}\text{Se}_2$ ($A =$ Tl, K, Cs, Rb) [1,2] has raised a lot of attention because their unique Fermi surface (FS) topology without hole pocket [3–8] challenges the electron-hole quasinesting scenario as the main Cooper pairing force in the Fe-based superconducting materials [9]. However, due to the phase separation associated with Fe vacancy ordering [10,11] in $A_x\text{Fe}_{2-y}\text{Se}_2$, it is still unclear whether superconductivity in this compound is related to that of the other iron-based superconductors. Very recently, it has been found that the isostructural material TlNi₂Se₂ with two more electrons on the 3*d* shell shows superconductivity with $T_c = 3.7$ K [12]. In contrast to $A_x\text{Fe}_{2-y}\text{Se}_2$, x-ray diffraction results indicate that this system is homogeneous without Ni vacancy or phase separation, and stoichiometric TlNi₂Se₂ was confirmed by energy dispersive x-ray spectroscopy [12]. A large normal-state Sommerfeld coefficient has been attributed to heavy fermion behavior [12], and its square root relationship with magnetic field in the mixed state suggests *d*-wave pairing symmetry. On the other hand, thermal conductivity measurements suggest multiple nodeless superconducting gaps [13]. Therefore, it is crucial to determine the electronic structure of TlNi₂Se₂ to understand the nature of the reported heavy fermions in this material and to establish possible connections with other unconventional superconductors.

In this Rapid Communication, we present high-resolution angle-resolved photoemission spectroscopy (ARPES) results on TlNi₂Se₂. Photon energy dependent measurements reveal that the electronic structure exhibits three dimensionality, with four bands crossing the Fermi level (E_F). Our density functional theory (DFT) calculations, renormalized by a factor of 1.4, match the experimentally determined band structure very well, indicating weaker correlation effects in TlNi₂Se₂ than in its cousin $A_x\text{Fe}_{2-y}\text{Se}_2$ [3]. We reveal that the flat top of one of the bands (γ) exhibits an asymmetric back-bending feature resulting in a camelback shape near E_F at $k = (0,0,\pi)$, the Z point of the first Brillouin zone (BZ). This shape is captured by our DFT calculations and seems to be a general feature of transition-metal pnictides [14]. This γ band forms four small FS lobes around the Z point, and between the lobes four flat parts resulting in a van Hove singularity (VHS) near E_F are identified. This finding provides a natural explanation to the heavy-electrons feature inferred from electronic specific heat and the upper critical field measurements [12] in this weakly correlated system. Indeed, in TlNi₂Se₂ γ takes on a value of 40 mJ/mol K², which is six times larger than that of BaFe₂As₂ (5.6 mJ/mol K²) with stronger correlations (renormalization factor ∼3 [15]).

Large single crystals of TlNi₂Se₂ were grown by the self-flux method [12]. ARPES measurements were performed at SIS beamline of Swiss Light Source, and at the one-cubed ARPES end station of BESSY with circular polarized photons ranging 20–70 eV. The angular and energy resolutions were set to 0.2° and 5–10 meV, respectively. Clean surfaces for the ARPES measurements were obtained by cleaving crystals
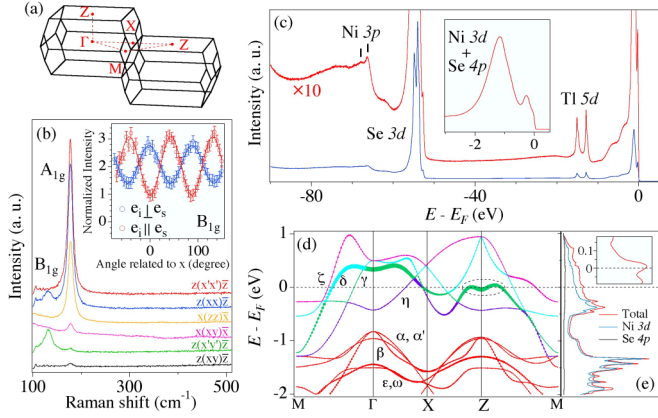
_____
*nan.xu@psi.ch
†ming.shi@psi.ch

FIG. 1. (Color online) (a) Two adjacent BZs of TlNi$_2$Se$_2$. (b) Raman spectra recorded under several polarization configurations [18]. (c) Core level spectra of TlNi$_2$Se$_2$ recorded with 150 eV photons. The inset is a close-up of the valence band near E_F. (d) DFT band structure plotted along high symmetry lines. The bands near E_F are colorized differently for a better visualization, and the linewidth indicates the Se 4p spectral weight. (e) DOS from DFT calculations.

in situ in a working vacuum better than 5×10^{-11} Torr. We label the momentum (k) values with respect to the 1 Ni/unit cell BZ, with the high symmetry points defined in Fig. 1(a). The Fermi level of the samples was referenced to that of a gold film evaporated onto the sample holder. Raman data have been recorded at room temperature using a 514.5 nm laser source and the single mode of a Horiba Jobin Yvon-T64000 micro-Raman spectrometer equipped with a CCD camera.

The Raman spectra in Fig. 1(b) show one A_{1g} mode (177.9 cm^{-1}) and one B_{1g} (132.8 cm^{-1}) phonon, similar to the observation on the isostructural 122-ferropnictides [16]. As illustrated in the inset, the intensity of these peaks is in perfect concordance with the fourfold symmetry of the crystal and the spectra are exempt of extra modes, which suggests that our TlNi$_2$Se$_2$ samples are not phase separated and do not show Ni vacancy ordering, in agreement with a previous study on KNi$_2$Se$_2$ [17].

Figure 1(c) shows the wide-energy photoemission spectra of TlNi$_2$Se$_2$. Clear double-peak features due to spin-orbit interaction are identified for states of Se 3d at binding energies (E_B) = 54.0 and 54.9 eV, Tl 5d at E_B = 12.9 and 15.1 eV, and Ni 3p at E_B = 66.3 and 67.9 eV (as shown in the inset). In Fig. 1(d), we plot the DFT band structure calculated for the experimental lattice parameters [12] and the height of Se from the Ni layer (z_{Se}) = 0.355 Å. Four bands cross E_F and exhibit non-negligible three dimensionality. The density of states (DOS) near E_F is contributed mainly by the Ni 3d states with a partial Se 4p spectral weight, as seen from Fig. 1(d) and the calculated DOS in Fig. 1(e). We notice that one specific band (γ) shows a back-bending camelback-shaped feature at the Z point [as shown in the dashed-line circle in Fig. 1(d)], leading to a flat band top sitting very close to E_F and contributing to a sharp peak in the DOS [inset of Fig. 1(e)]. This gives us a first indication that the heavy electrons reported in TlNi$_2$Se$_2$ may originate from this flat band top. This band results from the hybridization of the Ni-d_{xy} and Se-p_z orbitals and is a universal feature in transition-metal
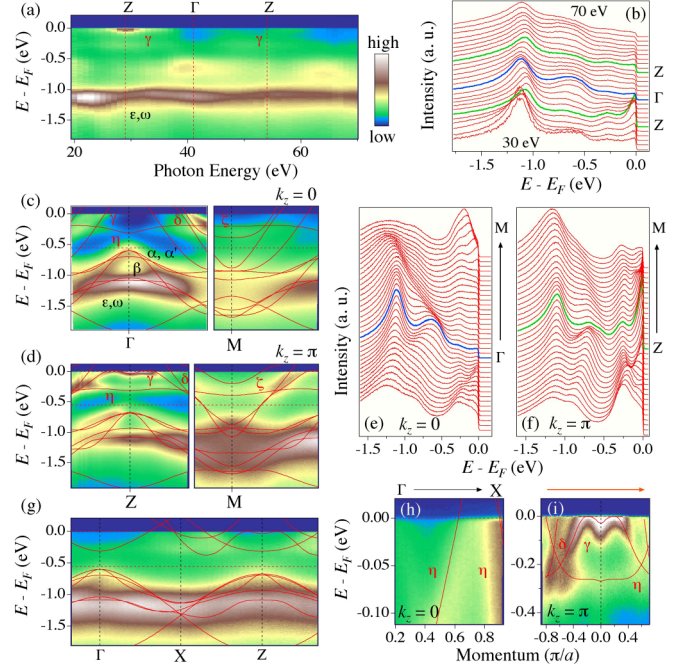

FIG. 2. (Color online) (a) Photon energy dependent ARPES intensity plot recorded at normal emission. (b) Corresponding EDC plot. (c), (d) ARPES intensity plot along the Γ-M and Z-M directions. DFT results renormalized by a factor 1.4 are overlapped. (e), (f) Corresponding EDC plots. (g) ARPES intensity plot along the Γ-X-Z momentum path, with renormalized DFT. (h) Near-E_F zoom along the Γ-X direction. (i) Same as (h), with the location in k space illustrated by the yellow arrow in Fig. 3(c).

pnictides and chalcogenides. The particular shape of its dispersion, with a back-bending feature near the Γ and Z points, is due to the combination of two opposite binding effects. Indeed, while the interaction of Ni-d_{xy} with Se-p_z is antibonding and causes the band to disperse upwards toward Z because of an increasing hybridization, the nearest-neighbor Ni-d_{xy}–Ni-d_{xy} interaction becomes bonding near this point, which explains the energy minimum. In most iron pnictides, the resulting saddle points are found in the unoccupied states [14], but the originality of TlNi$_2$Se$_2$ is that the Fermi level crosses it.

In Figs. 2(a) and 2(b), we plot normal emission ARPES intensities as a function of photon energy and their corresponding energy distribution curves (EDCs). Clear periodic variations of peak positions, especially for the γ band near E_F and the ϵ/ω band at $E_B \sim 1.2$ eV, are observed with tuning the k_z value by changing the photon energy, indicating strong three- dimensionality of the band structure in TlNi$_2$Se$_2$. Using the nearly-free electron approximation with an inner potential of 17 eV, we estimate $h\nu = 34$ eV for the $k_z = 0$ plane, and $h\nu = 29/54$ eV for the $k_z = \pi$ planes. We plot the ARPES intensity along the Γ-M and Z-M directions in Figs. 2(c) and 2(d), which are recorded with $h\nu = 34$ and 29 eV, respectively. The corresponding EDCs are shown in Figs. 2(e) and 2(f). At first sight, the overall band structure of TlNi$_2$Se$_2$ shows great similarity with BaFe$_2$As$_2$ [19] and BaCo$_2$As$_2$ [20]. The α, α', and β hole-like pockets centered at the Γ point in BaFe$_2$As$_2$ are fully filled in TlNi$_2$Se$_2$, with the bands topping ~ 0.6 eV below E_F. The γ
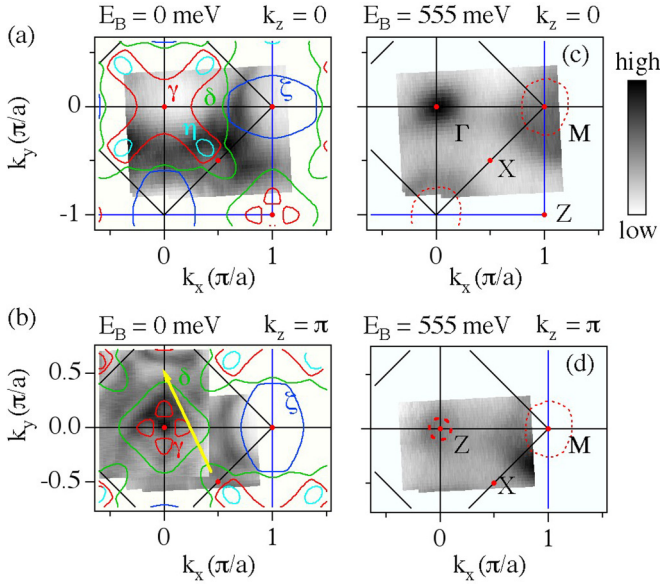
FIG. 3. (Color online) (a), (b) FS mappings for the $k_z = 0$ and π planes, respectively, obtained by integrating the ARPES intensity within $E_F \pm 5$ meV. (c), (d) Same as (a) and (b) but recorded 555 meV below E_F.

and δ electronlike pockets located at the M point in $BaFe_2As_2$ are more than half filled in $TlNi_2Se_2$ and form holelike pockets at the Γ point. One flat band (η) sits ~250 meV below E_F in $TlNi_2Se_2$, which is also observed near E_F in $BaCo_2As_2$ [20,21]. Besides all these states, the additional ζ band is observed in $TlNi_2Se_2$ around the M point. Our ARPES data suggest that $TlNi_2Se_2$ shares a universal band structure with $BaFe_2As_2$ and $BaCo_2As_2$, with a chemical potential shifted due to more $3d$ electrons in $TlNi_2Se_2$ ($3d^{8.5}$) than in $BaFe_2As_2$ ($3d^6$) and $BaCo_2As_2$ ($3d^7$). This is indeed what is expected from our DFT calculations, which match the experimental data very well with a renormalization factor of 1.4 as seen in Figs. 2(c) and 2(d). $TlNi_2Se_2$ can thus be viewed as heavily electron doped $TlFe_2Se_2$ ($3d^{6.5}$), as we will discuss more later.

Similarly, we plot the ARPES intensity along Γ-X-Z obtained with photon energy $h\nu = 54$ eV in Fig. 2(g), which also shows good agreement with the renormalized DFT calculations. In order to examine the details for the bands near E_F, high-resolution measurements have been recorded along Γ-X at the $k_z = 0$ plane ($h\nu = 41$ eV). As shown in Fig. 2(h), the holelike η band crosses E_F, with the intensity enhanced due to the matrix element effect. Similarly, Fig. 2(i) shows the band structure in the $k_z = \pi$ plane ($h\nu = 29$ eV), cutting slightly off the Z-X direction [as illustrated by the yellow arrow in Fig. 3(c)], in order to well separate the γ and δ bands. In agreement with DFT, the γ, δ, and η bands are observed, hybridizing with each other at their intersections.

In Figs. 3(a) and 3(b), we display the Fermi surface at $k_z = 0$ and π, respectively. The corresponding DFT calculations (with the chemical potential slightly shifted upward by 7 meV) are also overlapped. The Fermi surface contours are relatively broad due to the three dimensionality of the system. Nevertheless, the overall features of the intensity map agrees

with Fermi surface crossing expected by the calculations: the γ and δ bands, which form a pair of degenerate electronlike pockets at the M point in $A_xFe_{2-y}Se_2$ [3–6], become holelike pockets crossing E_F at the Γ point. The δ band crosses the Z point with a smaller k_F and the γ band creates four small lobes because of the back-bending feature discussed before. The η band forms a small holelike pocket near the X point, and the ζ band forms an electronlike pocket at the M point. In contrast, we find that the constant energy maps recorded at 550 meV below E_F for the $k_z = 0$ and π planes, which are, respectively, displayed in Figs. 3(c) and 3(d), are quite similar to the FSs of $A_xFe_{2-y}Se_2$, on which superconducting gaps are observed below T_c [6]. To illustrate this resemblance, we overlap on these figures the FSs obtained for $A_xFe_{2-y}Se_2$ in Ref. [6]. Similarly to the case of $BaFe_2As_2$ and $BaCo_2As_2$, $TlNi_2Se_2$ can be interpreted as a heavily electron doped $TlFe_2Se_2$ as a first approximation. Therefore, our results suggest that $TlFe_2Se_2$, the phase without vacancy ordering, is the superconducting compound of the iron-chalcogenide $Tl_xFe_{2-y}Se_2$, which is consistent with the scanning tunneling microscopy results [10] and supports the conclusions derived from previous ARPES experiments on $AFe_{2-x}Se_2$ [3–8].

The significant reduction of electron correlation strength in $TlNi_2Se_2$ (renormalization factor of 1.4) as compared to $TlFe_2Se_2$ (renormalization factor of 2.5 [3]) is anticipated due to the increased filling of the electronic $3d$ shell. Indeed, the stronger correlations in $BaFe_2As_2$ as compared to $BaCo_2As_2$ are driven by the lower band filling in the presence of strong Hund's coupling [20]. The mass enhancement due to correlation effects in $TlNi_2Se_2$ is much smaller than that deduced from the Sommerfeld coefficient [12]. Here we suggest the large Sommerfeld coefficient to be related to the flat band near the chemical potential at the Z point. As seen from the result in Fig. 4(c) and the corresponding EDC plot in Fig. 4(g), which is recorded at $T = 5$ K, the top of the γ band sits at the S point, ~2 meV below the E_F along the Z-X direction [C1 in Fig. 4(a)], and bends back with the band bottom at ~18 meV below the E_F [indicated by the EDC taken at the Z point shown in the inset of Fig. 4(g)]. Along the Z-M direction [C2 in Fig. 4(a)], the band top of γ is slightly above E_F, leading the γ band to double-cross E_F and forming small lobes. The γ band top along Z-M is estimated at ~15 meV above E_F from the high-temperature data (150 K) divided by the Fermi function shown in Fig. 4(i). In Fig. 4(e), we plot the ARPES intensity along the momentum path passing through the S point and perpendicular to the Z-X direction [C3 in Fig. 4(a)]. The corresponding EDC plot is also shown in Fig. 4(h). The γ band crosses E_F four times (passing through two small holelike lobes), and has a negative curvature at the S point along C1, as seen from Fig. 4(e), and the extracted band structure in Fig. 4(f). At the same time, the γ band has a positive curvature at the S point along the perpendicular direction C1 as shown in Figs. 4(c) and 4(d). Therefore, our data confirms the picture discussed before and, in particular, the camelback shape and the VHS at the S points. This can be better visualized in the band structure plotted in Fig. 4(b). In fact, this VHS is guaranteed by the asymmetry of the back-bending feature as shown in Fig. 4(c) and the extracted band structure in Fig. 4(d) along the X-Z-M direction.
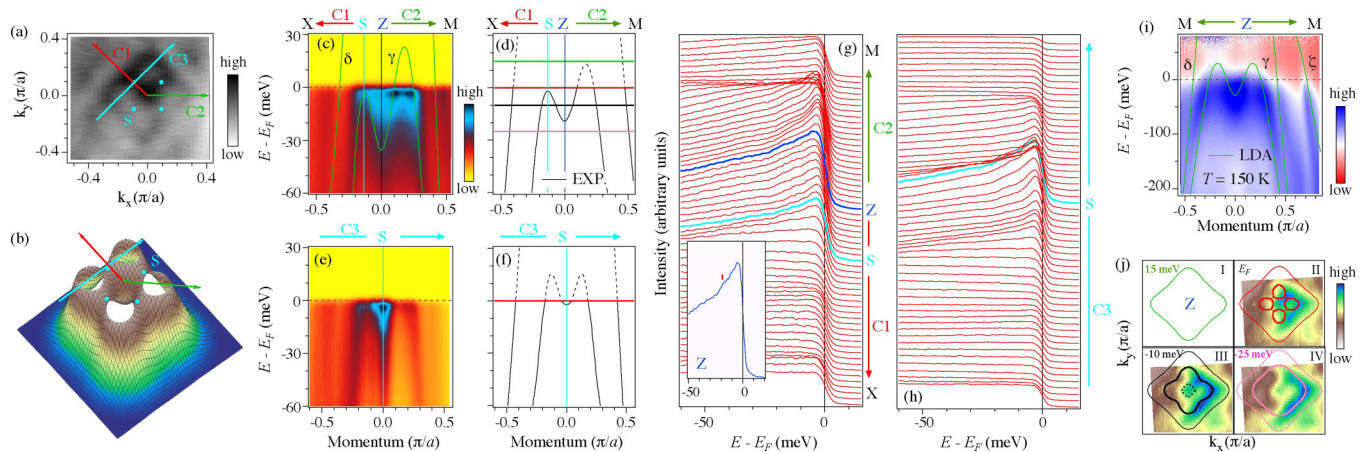
FIG. 4. (Color online) (a) FS plot near the Z point. (b) Illustration of the band structure near the Z point. (c) ARPES results along C1-C2. (d) Corresponding extracted band dispersion. (e), (f) Same as (c) and (d), but along C3. (g), (h) EDC plots for C1-C2 and C3. The inset in (g) is the EDC taken at the Z point. (i) ARPES intensity plot taken at $T = 150$ K. (j) Constant energy map contours taken near E_F.

The existence of VHS very close to E_F, provides a natural explanation for the large Sommerfeld coefficient in this weakly correlated system TlNi$_2$Se$_2$. In the meantime, the FS topology of the γ band changes dramatically when slightly tuning the chemical potential due to the VHS, as indicated in Fig. 4(j), I–IV. When we put the chemical potential > 15 meV above E_F, only the δ band crosses at the Z point and forms a holelike pocket. By putting the chemical potential at 2 meV $> E_B > -15$ meV, the γ band crosses the chemical potential but only along the Z-M directions, forming four small holelike lobes. When the chemical potential is setting in the range of 17 meV $> E_B > 2$ meV, the γ band crosses the chemical potential twice, both along the Z-M and Z-X directions, forming a small electronlike pocket inside a concentric holelike pocket. Further shifting the chemical potential down to $E_B > 17$ meV, the inner electron pocket disappears, leaving two holelike pockets at the Z point. All these Lifshitz transitions associated with VHS happen with the chemical potential varying by less than 30 meV, providing a possible explanation for why T_c of KNi$_2$Se$_2$ ($\sim$0.8 K) [22] is $\sim$4 times smaller than that of TlNi$_2$Se$_2$. Because K is much more sensitive to air than Tl, a slight shift of chemical potential in KNi$_2$Se$_2$ is expected. The difference of DOS near E_F due to this small chemical potential variation cannot explain $\sim$4 times smaller T_c in KNi$_2$Se$_2$. Most interestingly, since the strength of the hybridization of Ni-d_{xy} with the Se-p_z orbital controls the position of the saddle point with respect to E_F, the FS topology is highly sensitive to the height of the selenium atom over the Ni-Se plane. This may be related to the sudden T_c drop under pressure recently reported in TlNi$_2$Se$_2$ [23].

It is worth mentioning that the end member of the hole-doped BaFe$_2$As$_2$, the iron pnictide KFe$_2$As$_2$, shows some similarities with TlNi$_2$Se$_2$. A large Sommerfeld coefficient ($\sim$94 mJ/mol K^2) [24] and nodal superconductivity have been reported in KFe$_2$As$_2$ [25–28] and Ba$_{0.1}$K$_{0.9}$Fe$_2$As$_2$ [29]. A similar pressure effect has also been observed in KFe$_2$As$_2$ [26] and TlNi$_2$SeS [23] and recently a VHS has been observed in KFe$_2$As$_2$ [30]. The VHS observed in the present work not only reconciles heavy-electron behavior with weak electronic Coulomb correlations in superconducting TlNi$_2$Se$_2$, but also serves as a key to understand the unconventional properties in nickel- and iron-pnictide superconductors.

[1] J. G. Guo, S. F. Jin, G. Wang, S. C. Wang, K. X. Zhu, T. T. Zhou, M. He, and X. L. Chen, Phys. Rev. B **82**, 180520(R) (2010).

[2] M.-H. Fang, H.-D. Wang, C.-H. Dong, Z.-J. Li, C.-M. Feng, J. Chen, and H. Q. Yuan, Europhys. Lett. **94**, 27009 (2011).

[3] T. Qian, X.-P. Wang, W.-C. Jin, P. Zhang, P. Richard, G. Xu, X. Dai, Z. Fang, J.-G. Guo, X.-L. Chen, and H. Ding, Phys. Rev. Lett. **106**, 187001 (2011).

[4] Y. Zhang, L. X. Yang, M. Xu, Z. R. Ye, F. Chen, C. He, H. C. Xu, J. Jiang, B. P. Xie, J. J. Ying, X. F. Wang, X. H. Chen, J. P.

Hu, M. Matsunami, S. Kimura, and D. L. Feng, Nat. Mater. **10**, 273 (2011).

[5] D. X. Mou, S. Y. Liu, X. W. Jia, J. F. He, Y. Y. Peng, L. Zhao, L. Yu, G. D. Liu, S. L. He, X. L. Dong, J. Zhang, H. D. Wang, C. H. Dong, M. H. Fang, X. Y. Wang, Q. J. Peng, Z. M. Wang, S. J. Zhang, F. Yang, Z. Y. Xu, C. T. Chen, and X. J. Zhou, Phys. Rev. Lett. **106**, 107001 (2011).

[6] X.-P. Wang, T. Qian, P. Richard, P. Zhang, J. Dong, H.-D. Wang, C.-H. Dong, M.-H. Fang, and H. Ding, Europhys. Lett. **93**, 57001 (2011).

[7] Z.-H. Liu, P. Richard, N. Xu, G. Xu, Y. Li, X.-C. Fang, L.-L. Jia, G.-F. Chen, D.-M. Wang, J.-B. He, T. Qian, J.-P. Hu, H. Ding, and S.-C. Wang, Phys. Rev. Lett. **109**, 037003 (2012).

[8] X.-P. Wang, P. Richard, X. Shi, A. Roekeghem, Y.-B. Huang, E. Razzoli, T. Qian, E. Rienks, S. Thirupathaiah, H.-D. Wang, C.-H. Dong, M.-H. Fang, M. Shi, and H. Ding, Europhys. Lett. **99**, 67001 (2012).

[9] P. Richard, T. Sato, K. Nakayama, T. Takahashi, and H. Ding, Rep. Prog. Phys. **74**, 124512 (2011).

[10] W. Li, H. Ding, P. Deng, K. Chang, C. L. Song, K. He, L. L. Wang, X. C. Ma, J.-P. Hu, X. Chen, and Q.-K. Xue, Nat. Phys. **8**, 126 (2012).

[11] Z. Wang, Y. J. Song, H. L. Shi, Z. W. Wang, Z. Chen, H. F. Tian, G. F. Chen, J. G. Guo, H. X. Yang, and J. Q. Li, Phys. Rev. B **83**, 140505(R) (2011).

[12] H. Wang, C. Dong, Q. Mao, R. Khan, X. Zhou, C. Li, B. Chen, J. Yang, Q. Su, and M. Fang, Phys. Rev. Lett **111**, 207001 (2013).

[13] X. C. Hong, Z. Zhang, S. Y. Zhou, J. Pan, Y. Xu, H. Wang, Q. Mao, M. Fang, J. K. Dong, and S. Y. Li, Phys. Rev. B **90**, 060504(R) (2014).

[14] O. K. Andersen and L. Boeri, Ann. Phys. **523**, 8 (2011).

[15] P. Richard, K. Nakayama, T. Sato, M. Neupane, Y.-M. Xu, J. H. Bowen, G. F. Chen, J. L. Luo, N. L. Wang, X. Dai, Z. Fang, H. Ding, and T. Takahashi, Phys. Rev. Lett. **104**, 137001 (2010).

[16] A.-M. Zhang and Q.-M. Zhang, Chin. Phys. B **22**, 087103 (2013).

[17] N. Lazarević, M. Radonjić, M. Scepanović, H. Lei, D. Tanasković, C. Petrovic, and Z. V. Popović, Phys. Rev. B **87**, 144305 (2013).

[18] Here x' and y' are parallel to the Ni-Ni bounding while x and y are at 45° from these axes. The inset shows the evolution of the Raman intensity of the B_{1g} mode as a function of the angle between the incident polarization e_i and the x axis, for e_i parallel and perpendicular to the scattered light polarization e_s.

[19] H. Ding, K. Nakayama, P. Richard, S. Souma, T. Sato, T. Takahashi, M. Neupane, Y.-M. Xu, Z.-H. Pan, A. V. Fedorov, Z. Wang, X. Dai, Z. Fang, G. F. Chen, J. L. Luo, and N. L. Wang, J. Phys.: Condens. Matter **23**, 135701 (2011).

[20] N. Xu, P. Richard, A. van Roekeghem, P. Zhang, H. Miao, W.-L. Zhang, T. Qian, M. Ferrero, A. S. Sefat, S. Biermann, and H. Ding, Phys. Rev. X **3**, 011006 (2013).

[21] R. S. Dhaka, Y. Lee, V. K. Anand, D. C. Johnston, B. N. Harmon, and A. Kaminski, Phys. Rev. B **87**, 214516 (2013).

[22] J. R. Neilson, A. Llobet, A. V. Stier, L. Wu, L. J. Wen, J. Tao, Y. Zhu, Z. B. Tesanovic, N. P. Armitage, and T. M. McQueen, Phys. Rev. B **86**, 054512 (2012).

[23] S. K. Goh, H. C. Chang, P. Reiss, P. L. Alireza, Y. W. Cheung, S. Y. Lau, Hangdong Wang, Qianhui Mao, Jinhu Yang, Minghu Fang, F. M. Grosche, and M. L. Sutherland, Phys. Rev. B **90**, 201105(R) (2014).

[24] M. Abdel-Hafiez, S. Aswartham, S. Wurmehl, V. Grinenko, C. Hess, S.-L. Drechsler, S. Johnston, A. U. B. Wolter, B. Büchner, H. Rosner, and L. Boeri, Phys. Rev. B **85**, 134533 (2012).

[25] J.-Ph. Reid, M. A. Tanatar, A. Juneau-Fecteau, R. T. Gordon, S. René de Cotret, N. Doiron-Leyraud, T. Saito, H. Fukazawa, Y. Kohori, K. Kihou, C. H. Lee, A. Iyo, H. Eisaki, R. Prozorov, and L. Taillefer, Phys. Rev. Lett. **109**, 087001 (2012).

[26] F. F. Tafti, A. Juneau-Fecteau, M.-È. Delage, S. René de Cotret, J.-Ph. Reid, A. F. Wang, X.-G. Luo, X. H. Chen, N. Doiron-Leyraud, and L. Taillefer, Nat. Phys. **9**, 349 (2013).

[27] M. A. Tanatar, J.-Ph. Reid, H. Shakeripour, X. G. Luo, N. Doiron-Leyraud, N. Ni, S. L. Bud'ko, P. C. Canfield, R. Prozorov, and L. Taillefer, Phys. Rev. Lett. **104**, 067002 (2010).

[28] T. Sato, K. Nakayama, Y. Sekiba, P. Richard, Y.-M. Xu, S. Souma, T. Takahashi, G. F. Chen, J. L. Luo, N. L. Wang, and H. Ding, Phys. Rev. Lett **103**, 047002 (2009).

[29] N. Xu, P. Richard, X. Shi, A. van Roekeghem, T. Qian, E. Razzoli, E. Rienks, G.-F. Chen, E. Ieki, K. Nakayama, T. Sato, T. Takahashi, M. Shi, and H. Ding, Phys. Rev. B **88**, 220508(R) (2013).

[30] D. L. Fang, X. Shi, Z. Y. Du, P. Richard, H. Yang, X. X. Wu, P. Zhang, T. Qian, X. X. Ding, Z. Y. Wang, T. K. Kim, M. Hoesch, A. F. Wang, X. H. Chen, J. P. Hu, H. Ding, and H.-H. Wen, arXiv:1412.0945.